10-2018

Ion-Sensitive Field-Effect Transistors With Micropillared Gates for Measuring Cell Ion Exchange at Molecular Levels

Mohammad G. Abdallah

Rayan Khan

Christian Garcia
The University of Texas Rio Grande Valley

Young-Tae Kim

Samir M. Iqbal
The University of Texas Rio Grande Valley

Recommended Citation

Abdallah, Mohammad G., Rayan Khan, Christian Garcia, Young-Tae Kim, and Samir M. Iqbal. 2018. "Ion-Sensitive Field-Effect Transistors With Micropillared Gates for Measuring Cell Ion Exchange at Molecular Levels." IEEE Access 6: 72675–82. https://doi.org/10.1109/ACCESS.2018.2874274.

IEEE Access
Multidisciplinary | Rapid Review | Open Access Journal

Received August 17, 2018, accepted September 18, 2018, date of publication October 8, 2018,
date of current version December 19, 2018.

Digital Object Identifier 10.1109/ACCESS.2018.2874274

Ion-Sensitive Field-Effect Transistors With Micropillared Gates for Measuring Cell Ion Exchange at Molecular Levels

MOHAMMAD G. ABDALLAH[1], RAYAN KHAN[2], CHRISTIAN GARCIA[3], YOUNG-TAE KIM[4,5], AND SAMIR M. IQBAL[6], (Senior Member, IEEE)

[1]Nano-Bio Lab, Department of Electrical Engineering, and the Nanotechnology Research Center, The University of Texas at Arlington (UT-Arlington), Arlington, TX 76019, USA
[2]Department of Biology, UT-Arlington, Arlington, TX 76013, USA
[3]Nano-Bio Lab and Department of Electrical Engineering, The University of Texas Rio Grande Valley (UTRGV), Edinburg, TX 78539, USA
[4]Department of Bioengineering, UT-Arlington, Arlington, TX 76010, USA
[5]Department of Urology, University of Texas Southwestern Medical Center at Dallas, Dallas TX 75390, USA
[6]Department of Electrical Engineering and the School of Medicine, UTRGV, Edinburg, TX 78539, USA

Corresponding author: Samir M. Iqbal (smiqbal@ieee.org)

This work was supported in part by the Offices of the Vice President of Research at The University of Texas at Arlington and the Dean of the College of Engineering and Computer Science at the University of Texas Rio Grande Valley.

ABSTRACT The detection of small concentrations of cancer cells before cancer takes over the primary organ completely, or metastasizes to other areas of the body is important for early screening of cancer. One approach to address cancer early screening is through cell ion exchange bioelectricity, which characterizes voltage potential in non-neuronal cells to regulate shape changing, proliferation, differentiation, migration, and cancer formation. Herein, novel ion-sensitive field-effective transistor (ISFET) modality is shown to measure cell behavior during the change of cell properties at molecular levels. ISFETs produce low resistance signals and consume low power. The small size of ISFETs enables miniature diagnosis devices that can be affordably fabricated in a massive array format. A large number of cells can be measured in parallel. Therefore, ISFET allows the combination of low sample requirements and prompt response. ISFETs have the ability to measure the effect of ions from complex biological samples and can be used as affordable point of care devices.

INDEX TERMS Cancer, biological interactions, cellular biophysics, biochemical analysis, diseases.

I. INTRODUCTION

In the United States and worldwide, cancer has become a major public health concern. In 2018, about 1,735,350 cancer cases are expected to be diagnosed in just the United States, with an estimated cancer mortality of 609,640. There is a medical necessity to enhance early cancer screening approaches so the treatment for cancer patients can be feasible in the early stages of cancer. In the early stages, there are more chances that cancer is not spread to other parts of the patient's body. Each cell class has a distinguishing profile based on its mechano-physical properties [1]. Cells are active microstructures arranged in a coherent formation. Cells contain certain concentrations of components like water, organic, and inorganic molecules. The organic molecules include nucleic acids, proteins, and lipids. Sodium, potassium, magnesium, calcium, chloride, phosphate and bicarbonate ions are examples of inorganic compounds. In addition, cells can handle incoming information signals using parallel cellular pathways. The activation of signaling is according to the types of inputs from physical or chemical stimuli. For cancer screening, measuring cells' accurate physical, chemical, electrical, and biological properties is essential for cancer patients.

A cell is a charged entity. In 1971, Cone theorized a general correlation between the proliferation of a cell and its membrane potential (V_m) [2]. The resting potential of cell membrane differs from cell to cell and fluctuates from -100 mV to -20 mV. Bioelectricity of the cell is controlled by K^+, Na^+, Cl^-, and Ca^{+2} ion channels [3]. The ion channels regulate key cell behaviors such as proliferation, cancer initiation, and progression [4]–[6]. These ion channels have been identified as fundamental parameters in cancer pathology. The measurements of V_m can be used to detect and identify tumor cells.

The microscale and nanoscale environments are known to modulate cellular behavior [8]. The micropatterned

and nanopatterned engineered surfaces have demonstrated the influence of topography on a variety of cellular functions, like the migration of endothelial cells and fibroblasts [9], [10], osteogenic differentiation of stem cells [11]–[14], mechano-sensitive gene expressions in fibroblast cells [15]–[18], directional polarization of neurons [19]–[24], and immobilization of tumor cells [25], [26]. Researchers have utilized micro/nanostructures and nanotextured surfaces for various applications to modulate the cellular responses. Small diameter nanowires with high aspect ratios are known to penetrate the cell membrane. Therefore, these have been used for applications requiring intracellular access, such as for drug delivery [27]–[32]. Silicon micropillar arrays have been used for the efficient isolation and capture of circulating tumor cells through enhanced local topographic interactions [33], [34].

Ion-selective field effect transistors (ISFETs) have been used to detect methylated nucleotides in a DNA sample, which is a critical step in tumorigenesis for most types of cancers [7]. Here, we introduce an ISFET semiconductor sensor device to report the changes in cell ion exchange at the molecular levels, and in particular the enhanced ion exchange that occurs during the diseased cell proliferation. Ion flux triggers the proliferation process so that cells can divide, differentiate, or die (Fig. 1(a)). The surface engineering approach with 3D features enhances the device's electrical properties in comparison to a flat surface device. Introducing an innovative surface with 3D micropillars at gate area improved the tumor cell detection. The modification on the gate thus lowered the transistor threshold voltage. Therefore, cancer cell molecular bioelectricity could be used to turn the device ON easily. The transistor channel length and width were 10 μm $\times$ 15 μm such as to hold only single cell at a given time. An array of micropillars in the channel length would capture single cell on top of the transistor gate without penetrating the cell. The array of silicon dioxide micropillars was simulated on top of the doped silicon channel area and two diameters for micropillars were used. Two diameters of the micropillars were chosen such that these sizes were not too wide to impede the free-flowing ions from reaching the gate area and not too thin that they would penetrate the cell wall. The effects of the micropillars' physical diameters on the device performance were also studied.

The cells were modeled to be on top of the micropillars, while the spaces around micropillars were filled with biological buffer. This allowed unimpeded ion exchange between the cell membrane and extracellular environment. The ions migrated to the cell outside surface and accumulated on the surface. The uneven distribution of ions between intracellular and extracellular environment created a potential difference across the cellular membrane. The measurements of cell ion exchange at the molecular level were affected by the cell membrane potential. The micropillar surface engineered gate enhanced the sensitivity of ISFET and made it suitable for measuring tumor cells in a simultaneous screening environment.

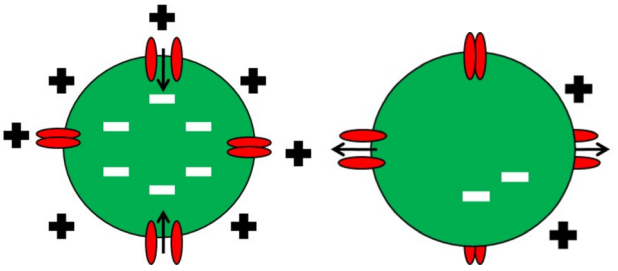

(a)

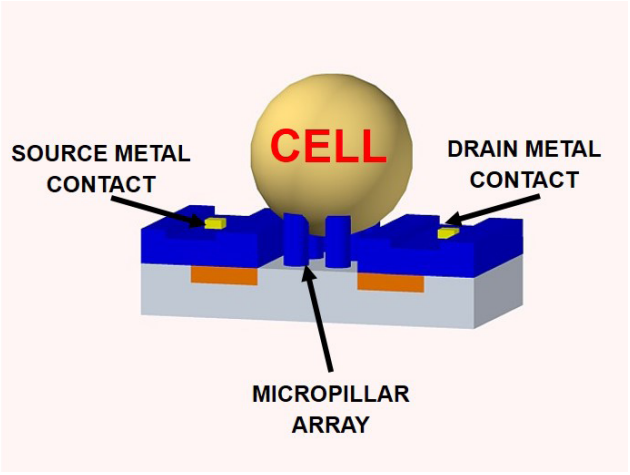

(b)

FIGURE 1. ISFET with micropillared gates. (a) Schematic illustration of cell ion channels. Cells are depolarized or hyperpolarized (b) 3D schematic of ISFET device. This shows a cell on top of micropillar array.

II. METHODS AND PROCEDURES

A. CELL TRANSMEMBRANE POTENTIAL

The voltage difference between inside and outside of a cell exists due to cell wall selective permeability of different ions. The Goldman–Hodgkin–Katz equation (1) below shows that the V_m depends on the permeabilities (P), and the intracellular and extracellular concentrations of major ions [35], [36]:

$$V_m = \frac{RT}{F}\ln\left(\frac{P_{Na}\left[Na^+\right]_o + P_K\left[K^+\right]_o + P_{Cl}\left[Cl^-\right]_o}{P_{Na}\left[Na^+\right]_i + P_K\left[K^+\right]_i + P_{Cl}\left[Cl^-\right]_i}\right) \quad (1)$$

where R is ideal gas constant, T is temperature and F is Faraday constant. The brackets with subscripts define the concentration of specific ions inside (i) or outside (o) the cell membrane. The concentrations of respective ions can be several orders of magnitude different across the cell membrane.

The cell cycle distinguishes into phases and one of the most significant factors that regulate cell cycle is the membrane potential (V_m) [4], [37]. As a result of ion channel and ion transport activities, the V_m of a resting cell is negative. The cells are said to be depolarized when the V_m is altered to relatively less negative state, whereas the cells are said to be hyperpolarized when the membrane potential is moved to more negative values than the resting membrane potential [38].

Direct in vitro and in vivo comparisons of V_m levels between normal and cancerous breast cells [39], hepatocytes and hepatocellular carcinoma cells [40], [41], normal and neoplastic adrenocortical tissues [42], and between normal and cancerous ovarian tissues have shown that cancer cells tend to be more depolarized than their normal counterparts [43].

B. ISFET MODEL

The COMSOL Multiphysics® Modeling Software was used to build the 3D geometric model (Fig. 1(b)). The silicon substrate was defined to be n-type with a donor concentration of $1.5 \times 10^{16}/\text{cm}^3$. The model terminals (source and drain) were designated as p-type doping with a concentration of $1 \times 10^{18}/\text{cm}^3$. The electrostatic model was represented by two terminals for source and drain. The source terminal voltage was set to zero. The drain terminal was set to -10 mV. A third terminal was used to apply the voltage at the gate area and at the edges of the micropillars to mimic cell membrane potential when the cell touched the micropillars. The semiconductor model was defined with two metal contacts on the source and drain (Fig. 2). The area with no micropillars between source-drain was separated from the channel by a thin 5 nm layer of silicon dioxide (SiO_2). A third metal contact was placed on that area to represent gate voltage. For the interface area between micropillar and the silicon substrate, a fourth metal contact was used to simulate the micropillars effect on the substrate.

C. VARIATION IN MICROPILLAR DIAMETER

In order to study the effect of physical parameters on the device performance, the diameters of the micropillars were varied. First, a 2 μm diameter was modeled and simulated. Next, 1 μm diameter was modeled and simulated. The simulations provided the DC electrical characteristics of both devices.

D. ELECTROSTATIC POTENTIAL

Both semiconductor and electrostatic models were executed simultaneously to simulate the DC characteristics of ISFET with the effects of electrostatic potential from the micropillars. The device turn-on voltage was determined by plotting the drain current. A low voltage of -10 mV was applied to the drain terminal. The voltages at the gate and edges of the micropillars (device surface) were swept from -200 mV to $+100$ mV. Then, drain voltage was swept from -100 mV to 0 mV while the surface voltage was swept from -200 mV to -100 mV. A plot of drain current versus drain voltage was generated with several values of surface voltage (i.e. voltage at the gate and edges of the micropillars). The electrostatic model captured the capacitor effect from SiO_2 micropillars, where the silicon substrate was grounded. The scalar electrical potential (V_{ES}) satisfied Poisson's equation.

The carriers' charges were solved by semiconductor model. From Poisson's equation (2), the left-side term shows electric field value. The right-side term shows the space

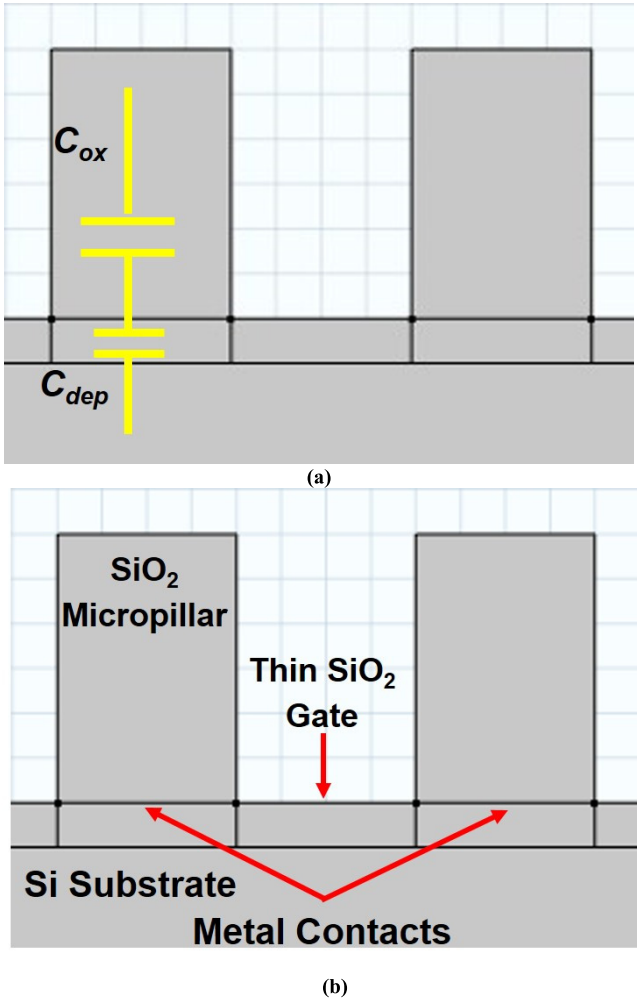

FIGURE 2. The boundary condition of model. (a) Ideal MOS capacitor (b) Metal contact boundary in semiconductor model

charge densities, where $\boldsymbol{q}$ is the charge of the carrier, and the electron and hole surface concentrations are denoted by $\boldsymbol{n}$ and $\boldsymbol{p}$, respectively. $\boldsymbol{N_a^-}$ and $\boldsymbol{N_d^+}$ are the acceptor and donor ion concentrations. At the steady state, the total charge contributions of the carriers can be calculated from the following:

$$\nabla.(-\epsilon \nabla V_{Semi}) = q\left(p - n + N_d^+ - N_a^-\right) \tag{2}$$

E. CHARGE DISTRIBUTION

Fig. 2(a) shows the boundary conditions for the model. The ideal MOS capacitor is modeled as SiO_2 micropillar. The silicon substrate under micropillars had equivalent charges as in the defined metal contact at the interface between Si-SiO_2. This resulted in a very narrow charge distribution near the interface at accumulation and inversion modes. At the depletion modes, the charges resulted in a depletion width (W_{dep}). Hence, the hole concentration near the interface equaled the donor concentration. This entailed:

$$\frac{1}{C} = \frac{1}{C_{ox}} + \frac{1}{C_{dep}} \tag{3}$$

$$\frac{1}{C_{dep}} = \frac{W_{dep}}{\varepsilon \times Area} \tag{4}$$

$$p_{interface} = N_d = n_i e^{[\frac{E_{i-interface}-E_f}{kT}]} = n_i e^{[\frac{E_f-E_i}{kT}]} \tag{5}$$

These metallic contacts were placed in the semiconductor model between Si-SiO_2 boundaries to mimic the electrical potential caused by the SiO_2 micropillar's capacitor effect (Fig. 2(b)). The metal contact voltage was set to be the voltage output from the electrostatic model solution ($V = V_{ES}$). The silicon substrate area under SiO_2 pillar was doped with p-type doping. The electrical insulation was assumed throughout the device boundary.

III. RESULTS AND DISCUSSION

The simulation results were plotted to obtain DC characteristics of the ISFET sensor. At the end of the simulation, the data clearly indicated membrane potential changes at the interfaces of the micropillars.

A. ISFET DC CHARACTERISTICS

The ISFET working principle is based on the monitoring of the changes of surface charges at the interface of the insulator and the overlying layer. This was mimicked by the applied voltage. The change in surface charges resulted in work function change that in turn was measured as a shift in the transistor threshold voltage. Fig. 3 shows the device electric potential for 2 μm × 3 μm and 1 μm × 3 μm array of micropillars. The electrical field is depicted by the arrow lines. By applying Poisson's equation at the SiO_2 micropillars, and by design, there are no charges in the SiO_2:

$$\frac{dE_{oxide}}{dx} = \rho = 0, \quad E_{oxide} = \text{constant} \tag{6}$$

$$V_{ES}(x, y) = \int E_{oxide-x} dx + \int E_{oxide-y} dy \tag{7}$$

The electrical potential changed linearly for both cases, where it was going away from the micropillars. The maximum electric potential was seen at the device gate and Si-SiO_2 boundary. The ISFET design allowed the achievement of a physiological response to ion exchange activity (cell molecular bioelectricity) toward cancer cell characterization. The micropillar diameter impacted the electric field direction as shown in Fig. 3. The 2 μm diameter micropillar shows electrical field direction covering the entire micropillars. However, 1 μm diameter shows electric field direction in only part of the micropillar for the same conditions ($V_d = -10$ mV, $V_g = -100$ mV). Micropillar diameter imposes a higher effect on the electric field when in contact with cells. The 2 μm × 3 μm device shows a higher electrical field effect than that for 1 μm × 3 μm device.

Fig. 4(a) shows the ISFET drain current with respect to the surface voltage at a low constant drain voltage of −10 mV for both 2 μm × 3 μm and 1 μm × 3 μm devices. The threshold voltage (V_T) of the devices was extracted from a log scale plot of $I_d - V_g$ by plotting and extrapolating to find V_T (Fig. 4 (b)).

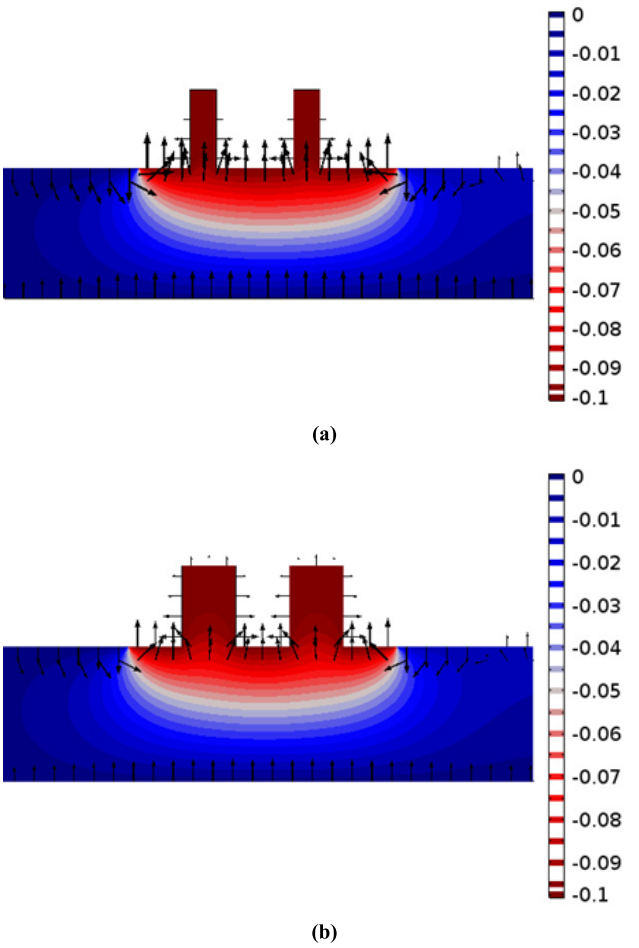

FIGURE 3. Device electrical potential results with micropillar sizes of (a) 1 μm × 3 μm, and (b) 2 μm × 3 μm. The color depicts the electrical potential magnitude as depicted on the color scale on the right. Arrows depict electrical field direction in x-y direction.

TABLE 1. ISFET DC characteristics summary.

Device (Diameter x Height)	V_T (mV)	I_{dsat} (nA)	g_m (μS)
2 μm x 3 μm	-90	0.96	10.62
1 μm x 3 μm	-140	0.85	6.06
No Micropillar	-10	0.04	4.00

The I_{dsat} was extracted from $I_d - V_d$ graph where ($V_g < V_T$, $V_d < V_g + |V_T|$) (Table 1).

The micropillar diameters showed a correlation with V_T and I_{dsat}. The V_T of the device was lower when the micropillar diameter was larger, which increased the drain channel current. The effective length of the device gate changed as the micropillar diameter changed. The effective gate length was 6 μm and 8 μm for the 2 μm × 3 μm and 1 μm × 3 μm device, respectively. The micropillar diameter controlled the device turn on/off voltage.

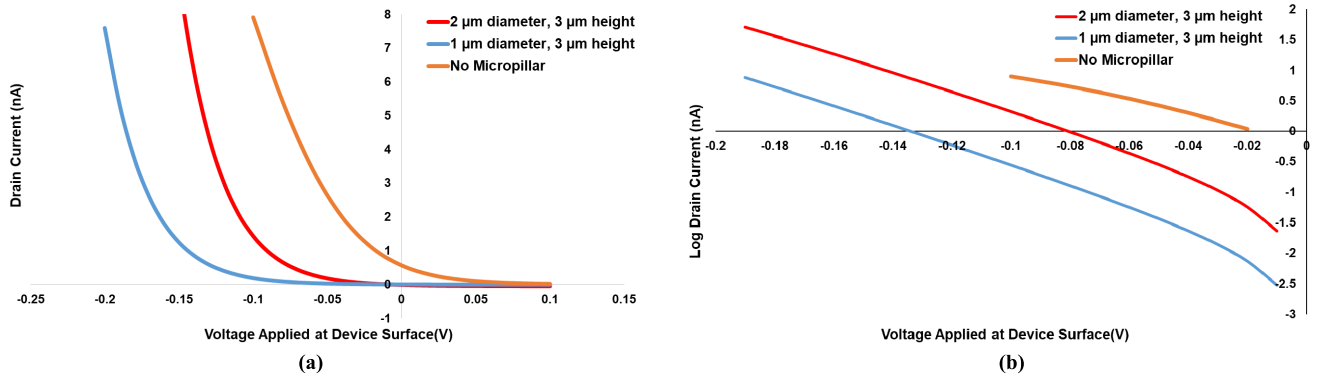

FIGURE 4. Drain current vs. surface voltage ($V_d = -10$ mV). (a) Linear plot, and (b) Drain current plotted in log scale to extract V_T.

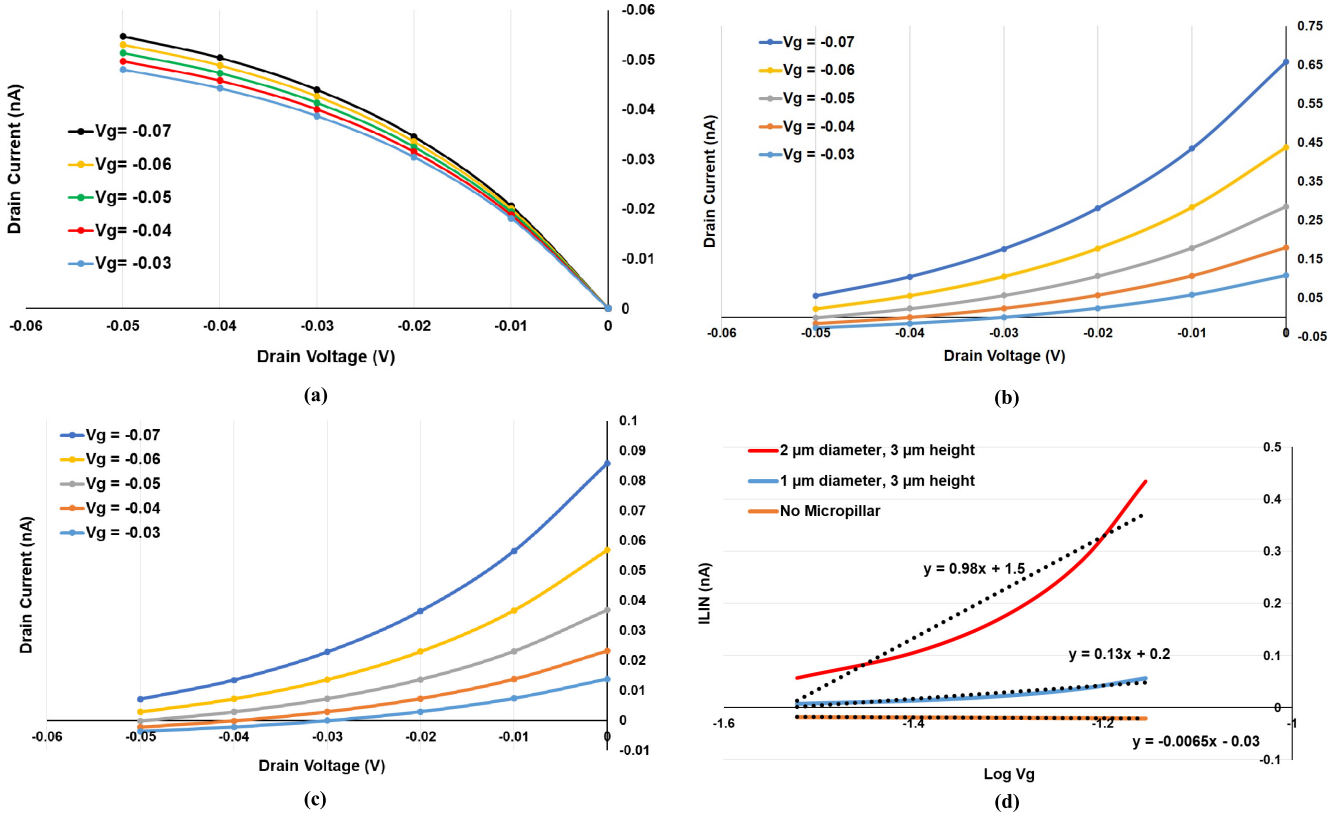

FIGURE 5. Drain current vs. drain voltage simulation analysis. (a) Drain current vs. drain voltage without micropillar effect (b) Drain current vs. drain voltage for device with 2 μm × 3 μm micropillar (c) Drain current vs. drain voltage for device with 1 μm × 3 μm (d) I_{LIN} vs. log values of the voltage applied to device surface micropillar and gate.

B. DRAIN CURRENT VS. DRAIN VOLTAGE WHILE RAMPING V_g

The drain current versus drain voltage simulation of ISFET without the effect of micropillars is shown in Fig. 5(a). The linear current (I_{LIN}) value was described as the drain current that passed through the device at $V_d = -10$ mV. The I_{LIN} was extracted from the plot of the drain current at ($V_d = -10$ mV) versus the surface voltage. A device sensitivity of 6.5 pA/dec was seen between -70 mV and -30 mV.

For the two SiO_2 micropillar diameters used in this simulations, the drain current output curves were recorded at different surface voltages (Figs. 5(b), 5(c)). With decreasing surface voltage, the output curves changed to the positive drain current through the device. Also, the micropillared devices showed an increase in drain current as the voltage amplitude $|V_d|$ decreased as a result of the coupling of the semiconductor and electrostatics models. The two models were executed concurrently to capture the micropillar electrostatic effect on FET.

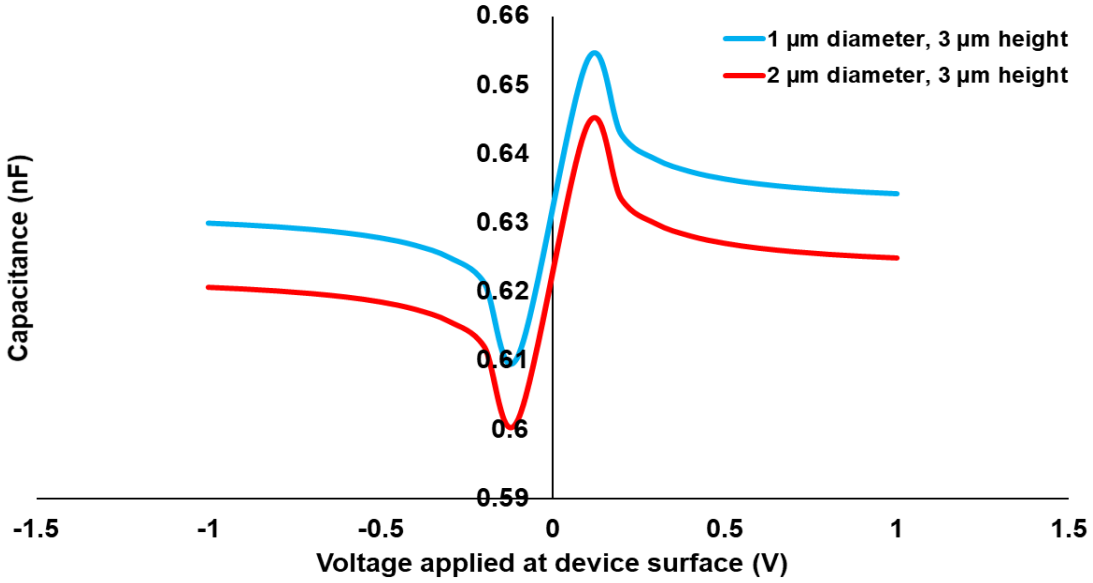

FIGURE 6. Device simulated capacitance behavior vs. surface voltage. Redline depicts the data for the 2 μm × 3 μm micropillar device, and the blue line shows the behavior of the 1 μm × 3 μm micropillar device.

To quantify the sensitivity of the devices, the linear currents were extracted from the curves. The value of I_{LIN} was 0.98 nA/dec and 0.13 nA/dec for 2 μm and 1 μm diameter micropillars, respectively (Fig. 5(d)).

The results showed that introducing the micropillar increased the device sensitivity (I_{LIN}). The current was higher when the diameter was larger. Here, a 2 μm diameter showed ~7.5 times more I_{LIN} than that for 1 μm diameter micropillars.

The limit of detection (LOD) of a device can be defined as:

$$\text{LOD} = \frac{3\sigma}{S} \tag{8}$$

where S is the sensitivity, σ is the standard deviation of the device current with no micropillar. The LOD of devices with no micropillars, 2 μm micropillars and 1 μm micropillars was 43 mV, −2 mV and −0.3 mV, respectively.

C. CAPACITANCE-VOLTAGE (C–V) CHARACTERISTICS

The C-V measurements of MOS capacitor structure provided device information. The MOS structure was modeled as a series connection of two capacitors: capacitance of the oxide and capacitance of depletion layer (3). The device capacitance depended on three operating modes: accumulation capacitance, which was oxide capacitor with no depletion layer, depletion capacitance, which was equal to the series connection of oxide and depletion layer capacitance, and inversion capacitance which became independent of the surface voltage.

For this simulation, all metal contacts were set to ground and the surface voltage was swept from −1 V to +1 V to record device capacitance from gate to bulk. The device capacitance behavior was recorded for the two micropillar diameters. The results showed that the capacitance depended on the micropillar diameters (Fig. 6). When micropillar diameter increased, device capacitance lowered. Accordingly, the device flat band voltage changed, and we captured the change in V_T.

The 2 μm × 3 μm device capacitance simulation showed lower capacitance when compared to 1 μm × 3 μm device and this described lower $|V_T|$.

D. CARRIER CONCENTRATIONS

The simulation showed no channel was formed between drain and source at $T = 0$. When surface voltage became positive, the silicon substrate showed electron accumulation in the silicon substrate channel area. The electron concentration in the channel area increased as the surface voltage increased and the device operated in accumulation mode: n-type became

TABLE 2. Carrier concentrations under the micropillars.

Gate Voltage (mV)	Electron Concentration (Log Values)	Hole Concentration (Log Values)
100	10.82	10.71
80	10.58	10.79
60	10.37	10.90
40	10.17	11.06
20	10.00	11.25
-20	9.76	11.73
-40	9.69	12.02
-60	9.65	12.32
-80	9.62	12.63
-100	9.61	12.94

more ''n''. Similarly, the positive charges gathered in silicon substrate channel area when surface voltage got negative. The electron concentration in the channel area decreased and the device operated in depletion mode. At $V_g \ll 0$, the drain current was generated equal to the total charge in the inversion layer. Therefore, hole concentration increased as the applied surface voltage on the device became more negative. At the end of the simulation, the carrier concentrations of the channel area (beneath SiO_2 micropillars) were extracted from the model. Table. 2 shows carrier concentrations versus the applied surface voltage. The hole concentration increased as applied potential became negative, which is shown from charge model (5). The electrons in channel area were exchanged by holes and formed an inversion channel of holes from source-drain.

IV. CONCLUSION

A simulation of measuring cell membrane voltage potential has been done on the ISFET devices with micropillars in the gate area. The simulation of the micropillars physical diameter was done (2 μm $\times$ 3 μm and 1 μm $\times$ 3 μm). The change in the ISFET output current was measured as the voltage mimicking the cell membrane potential was applied to the device. The ISFET sensing principle related to the change in the device threshold current due to surface charges, which changed the operative voltage potential of the semiconductor channel. These surface charges would be contributed by the V_m of cell in a practical device. The cells would be sitting atop the micropillars. The micropillar diameters played a key role in controlling device DC characteristics and performance. An enhancement of device performance was observed for micropillar diameter of 2 μm. The results showed that cancer cell could be characterized by ISFET sensor, based on their enhanced ion concentrations in the solution. The simulations showed the enchantment of ISFET device sensitivity when micropillars were introduced. ISFETs can be manufactured at an economical price and would be cost-effective for point of care application.

ACKNOWLEDGMENT

The authors acknowledge useful discussions with Dr. M. R. Hassan, S. S. S. Peri, Dr. N. Mansur, and Dr. M. U. Raza. A number of life lessons were learnt from Dr. S. Kumar and his affiliates at the University of Texas Rio Grande Valley.

This paper was presented at the 2017 IEEE Sensors Conference at Glasgow, U.K., in 2017.

REFERENCES

[1] M. Islam, M. M. Bellah, A. Sajid, M. R. Hasan, Y.-T. Kim, and S. M. Iqbal, ''Effects of nanotexture on electrical profiling of single tumor cell and detection of cancer from blood in microfluidic channels,'' *Sci. Rep.*, vol. 5, Sep. 2015, Art. no. 13031.

[2] C. D. Cone, Jr., ''Unified theory on the basic mechanism of normal mitotic control and oncogenesis,'' *J. Theor. Biol.*, vol. 30, no. 1, pp. 151–181, 1971.

[3] V. R. Rao, M. Perez-Neut, S. Kaja, and S. Gntile, ''Voltage-gated ion channels in cancer cell proliferation,'' *Cancers*, vol. 7, no. 2, pp. 849–875, 2015.

[4] M. Yang and W. J. Brackenbury, ''Membrane potential and cancer progression,'' *Frontiers Physiol.*, vol. 4, p. 185, Jul. 2013.

[5] M. B. A. Djamgoz, R. C. Coombes, and A. Schwab, ''Ion transport and cancer: From initiation to metastasis,'' *Philos. Trans. Roy. Soc. B, Biol. Sci.*, vol. 369, no. 1638, p. 20130092, 2014.

[6] X. Huang and L. Y. Jan, ''Targeting potassium channels in cancer,'' *J. Cell Biol.*, vol. 206, no. 2, pp. 151–162, 2014.

[7] M. Kalofonou and C. Toumazou, ''Semiconductor technology for early detection of DNA methylation for cancer: From concept to practice,'' *Sens. Actuators B, Chem.*, vol. 178, pp. 572–580, Mar. 2013.

[8] D.-H. Kim, P. P. Provenzano, C. L. Smith, and A. Levchenko, ''Matrix nanotopography as a regulator of cell function,'' *J. Cell Biol.*, vol. 197, no. 3, pp. 351–360, 2012.

[9] X. Jiang, D. A. Bruzewicz, A. P. Wong, M. Piel, and G. M. Whitesides, ''Directing cell migration with asymmetric micropatterns,'' *Proc. Nat. Acad. Sci. USA*, vol. 102, no. 4, pp. 975–978, 2005.

[10] G. Mahmud *et al.*, ''Directing cell motions on micropatterned ratchets,'' *Nat. Phys.*, vol. 5, no. 8, pp. 606–612, 2009.

[11] R. McBeath, D. M. Pirone, C. M. Nelson, K. Bhadriraju, and C. S. Chen, ''Cell shape, cytoskeletal tension, and RhoA regulate stem cell lineage commitment,'' *Develop. Cell*, vol. 6, no. 4, pp. 483–495, 2004.

[12] E. Avizienyte and M. C. Frame, ''Src and FAK signalling controls adhesion fate and the epithelial-to-mesenchymal transition,'' *Current Opinion Cell Biol.*, vol. 17, no. 5, pp. 542–547, 2005.

[13] K. C. Popat *et al.*, ''Osteogenic differentiation of marrow stromal cells cultured on nanoporous alumina surfaces,'' *J. Biomed. Mater. Res.*, vol. 80A, no. 4, pp. 955–964, 2007.

[14] R. A. Gittens *et al.*, ''Differential responses of osteoblast lineage cells to nanotopographically-modified, microroughened titanium–aluminum–vanadium alloy surfaces,'' *Biomaterials*, vol. 33, no. 35, pp. 8986–8994, 2012.

[15] L. E. McNamara *et al.*, ''The role of microtopography in cellular mechanotransduction,'' *Biomaterials*, vol. 33, no. 10, pp. 2835–2847, 2012.

[16] M. J. Dalby, N. Gadegaard, M. O. Riehle, C. D. W. Wilkinson, and A. S. G. Curtis, ''Investigating filopodia sensing using arrays of defined nano-pits down to 35 nm diameter in size,'' *Int. J. Biochem. Cell Biol.*, vol. 36, no. 10, pp. 2005–2015, 2004.

[17] M. J. Dalby, M. O. Riehle, D. S. Sutherland, H. Agheli, and A. S. Curtis, ''Use of nanotopography to study mechanotransduction in fibroblasts–methods and perspectives,'' *Eur. J. Cell Biol.*, vol. 83, no. 4, pp. 159–169, 2004.

[18] M. J. Dalby, ''Topographically induced direct cell mechanotransduction,'' *Med. Eng. Phys.*, vol. 27, no. 9, pp. 730–742, 2005.

[19] A. M. Rajnicek, S. Britland, and C. McCaig, ''Contact guidance of CNS neurites on grooved quartz: Influence of groove dimensions, neuronal age and cell Type,'' *J. Cell Sci.*, vol. 110, no. 23, pp. 2905–2913, 1997.

[20] D. Y. Fozdar, J. Y. Lee, C. E. Schmidt, and S. Chen, ''Selective axonal growth of embryonic hippocampal neurons according to topographic features of various sizes and shapes,'' *Int. J. Nanomed.*, vol. 6, no. 1, pp. 45–57, 2010.

[21] N. Gomez, J. Y. Lee, J. D. Nickels, and C. E. Schmidt, ''Micropatterned polypyrrole: A combination of electrical and topographical characteristics for the stimulation of cells,'' *Adv. Funct. Mater*, vol. 17, no. 10, pp. 1645–1653, 2007.

[22] N. Gomez, S. Chen, and C. E. Schmidt, ''Polarization of hippocampal neurons with competitive surface stimuli: contact guidance cues are preferred over chemical ligands,'' *J. Roy. Soc., Interface*, vol. 4, no. 13, pp. 223–233, 2007.

[23] N. Gomez, Y. Lu, S. Chen, and C. E. Schmidt, ''Immobilized nerve growth factor and microtopography have distinct effects on polarization versus axon elongation in hippocampal cells in culture,'' *Biomaterials*, vol. 28, no. 2, pp. 271–284, 2007.

[24] A. Ferrari, M. Cecchini, M. Serresi, P. Faraci, D. Pisignano, and F. Beltram, ''Neuronal polarity selection by topography-induced focal adhesion control,'' *Biomaterials*, vol. 31, no. 17, pp. 4682–4694, 2010.

[25] S. Wang, Y. Wan, and Y. Liu, ''Effects of nanopillar array diameter and spacing on cancer cell capture and cell behaviors,'' *Nanoscale*, vol. 6, no. 21, pp. 12482–12489, 2014.

[26] S. Wang *et al.*, ''Three-dimensional nanostructured substrates toward efficient capture of circulating tumor cells,'' *Angew. Chem. Int. Ed. English*, vol. 48, pp. 8970–8973, Oct. 2009.

[27] X. Xie, A. M. Xu, S. Leal-Ortiz, Y. Cao, C. C. Garner, and N. A. Melosh, ''Nanostraw–electroporation system for highly efficient intracellular delivery and transfection,'' *ACS Nano*, vol. 7, no. 5, pp. 4351–4358, 2013.

[28] C. Chiappini, J. O. Martinez, E. De Rosa, C. S. Almeida, E. Tasciotti, and M. M. Stevens, "Biodegradable nanoneedles for localized delivery of nanoparticles *in vivo*: Exploring the biointerface," *ACS Nano*, vol. 9, no. 5, pp. 5500–5509, 2015.
[29] A. K. Shalek *et al.*, "Nanowire-mediated delivery enables functional interrogation of primary immune cells: Application to the analysis of chronic lymphocytic leukemia," *Nano Lett.*, vol. 12, no. 12, pp. 6498–6504, 2012.
[30] H. Persson *et al.*, "Fibroblasts cultured on nanowires exhibit low motility, impaired cell division, and DNA damage," *Small*, vol. 9, no. 23, pp. 4006–4016, 2013.
[31] A. K. Shalek *et al.*, "Vertical silicon nanowires as a universal platform for delivering biomolecules into living cells," *Proc. Nat. Acad. Sci. USA*, vol. 107, no. 5, pp. 1870–1875, 2010.
[32] J. VanDersarl, A. M. Xu, and N. A. Melosh, "Nanostraws for direct fluidic intracellular access," *Nano Lett.*, vol. 12, no. 8, pp. 3881–3886, 2011.
[33] F. Zhang *et al.*, "Hierarchical nanowire arrays as three-dimensional fractal nanobiointerfaces for high efficient capture of cancer cells," *Nano Lett.*, vol. 16, no. 1, pp. 766–772, 2016.
[34] S. Nagrath *et al.*, "Isolation of rare circulating tumour cells in cancer patients by microchip technology," *Nature*, vol. 450, pp. 1235–1239, Dec. 2007.
[35] D. E. Goldman, "Potential, impedance, and rectification in membranes," *J. Gen. Physiol.*, vol. 27, no. 1, pp. 37–60, 1943.
[36] A. L. Hodgkin and B. Katz, "The effect of sodium ions on the electrical activity of the giant axon of the squid," *J. Physiol.*, vol. 108, no. 1, pp. 37–77, 1949.
[37] D. J. Blackiston, K. A. McLaughlin, and M. Levin, "Bioelectric controls of cell proliferation: Ion channels, membrane voltage and the cell cycle," *Cell Cycle*, vol. 8, no. 21, pp. 3527–3536, 2009.
[38] S. H. Wright, "Generation of resting membrane potential," *Adv. Physiol. Educ.*, vol. 28, no. 4, pp. 139–142, 2004.
[39] A. A. Marmo, D. M. Morris, M. A. Schwalke, I. G. Iliev, and S. Rogers, "Electrical potential measurements in human breast cancer and benign lesions," *Tumor Biol.*, vol. 15, no. 3, pp. 147–152, 1994.
[40] R. Binggeli and I. L. Cameron, "Cellular potentials of normal and cancerous fibroblasts and hepatocytes," *Cancer Res.*, vol. 40, no. 6, pp. 1830–1835, 1980.
[41] D. Stevenson, R. Binggeli, R. C. Weinstein, J. G. Keck, M. C. Lai, and M. J. Tong, "Relationship between cell membrane potential and natural killer cell cytolysis in human hepatocellular carcinoma cells," *Cancer Res.* vol. 49, no. 17, pp. 4842–4845, 1989.
[42] J. Lymangrover, A. F. Pearlmutter, R. Franco-Saenz, and M. Saffran, "Transmembrane potentials and steroidogenesis in normal and neoplastic human adrenocortical tissue," *J. Clin. Endocrinol. Metabolism* vol. 41, no. 4, pp. 697–706, 1975. doi: 10.1210/jcem-41-.4-697.
[43] K. Redmann, V. Muller, S. Tanneberger, and W. Kalkoff, "The membrane potential of primary ovarian tumor cells in vitro and its dependence on the cell cycle," *Acta biologica et medica Germanica*, vol. 28, no. 5, pp. 853–856, 1972.

MOHAMMAD G. ABDALLAH was born in Kuwait in 1986. He received the B.S. degree in electrical engineering from The University of Texas at Arlington (UT-Arlington), Arlington, TX, USA, in 2012, and the Ph.D. degree from the Department of Electrical Engineering, UTA, under the supervision of Dr. S. M. Iqbal, in 2018.

He was a Graduate Research Associate with the Nano-Bio Lab, Nanotechnology Research Center, UTA. He is currently a Faculty Member with the College of Engineering, UT-Arlington. His research interests are in developing novel nano-bio interfaces for single cell analysis.

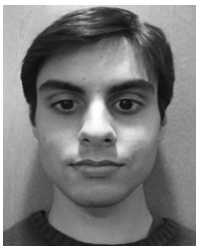

RAYAN KHAN was born in Richmond Hill, ON, Canada. He completed the high school at the Carroll Senior High School, Southlake, TX, USA, in 2015. He is currently pursuing the B.Sc. degree in biology at UT-Arlington. He has been an Undergraduate Research Associate with the Nano-Bio Lab under the supervision of Dr. S. M. Iqbal.

CHRISTIAN GARCIA was born in Brownsville, TX, USA. He graduated from the South Texas High School for Medical Professionals, Mercedes, TX, USA, in 2015. He is currently pursuing the B.Sc. degree in electrical engineering from the University of Texas Rio Grande Valley, Edinburg, TX, USA. He is also an Undergraduate Research Associate with the Nano-Bio Lab, under the supervision of Dr. S. M. Iqbal.

YOUNG-TAE KIM was born in Seoul, South Korea, in 1973. He received the B.S. degree in biomedical engineering from Yonsei University, South Korea, in 1999, and the Ph.D. degree from the Bioengineering Department, University of Utah, Salt Lake City, USA, in 2004. He was a Post-Doctoral Researcher at the Georgia Institute of Technology, Atlanta, USA, from 2004 to 2007.

He is currently an Associate Professor with the Bioengineering Department, UT-Arlington.

SAMIR M. IQBAL was born in Bahrain in 1972. He received the bachelor's degree in electrical engineering from the NED University of Engineering and Technology, Karachi, Pakistan, in 1997, and the Ph.D. degree from the School of Electrical and Computer Engineering, Purdue University, West Lafayette, IN, USA, in 2007.

He is currently a Professor with the Electrical Engineering Department and holds a joint appointment with the School of Medicine, UTRGV, Edinburg, TX, USA. He was a Faculty Member and the Presidential Research Fellow at UT-Arlington before he joined UTRGV as the Department Chair.